Large and seasonally varying biospheric CO_2 fluxes in the Los Angeles megacity revealed by atmospheric radiocarbon

John B. Miller[a,1], Scott J. Lehman[b], Kristal R. Verhulst[c], Charles E. Miller[c], Riley M. Duren[c,2], Vineet Yadav[c], Sally Newman[d,3], and Christopher D. Sloop[e,4]

[a]National Oceanic and Atmospheric Administration Global Monitoring Laboratory, Boulder, CO 80305; [b]Institute of Arctic and Alpine Research, University of Colorado, Boulder, CO 80309; [c]Jet Propulsion Laboratory, California Institute of Technology, Pasadena, CA 91109; [d]Division of Geological and Planetary Sciences, California Institute of Technology, Pasadena, CA 91125; and [e]Earth Networks, Germantown, MD 20876

Edited by Ronald C. Cohen, University of California, Berkeley, CA, and accepted by Editorial Board Member Akkihebbal R. Ravishankara August 7, 2020 (received for review March 20, 2020)

Measurements of $\Delta^{14}C$ and CO_2 can cleanly separate biogenic and fossil contributions to CO_2 enhancements above background. Our measurements of these tracers in air around Los Angeles in 2015 reveal high values of fossil CO_2 and a significant and seasonally varying contribution of CO_2 from the urban biosphere. The biogenic CO_2 is composed of sources such as biofuel combustion and human metabolism and an urban biospheric component likely originating from urban vegetation, including turf and trees. The urban biospheric component is a source in winter and a sink in summer, with an estimated amplitude of 4.3 parts per million (ppm), equivalent to 33% of the observed annual mean fossil fuel contribution of 13 ppm. While the timing of the net carbon sink is out of phase with wintertime rainfall and the sink seasonality of Southern California Mediterranean ecosystems (which show maximum uptake in spring), it is in phase with the seasonal cycle of urban water usage, suggesting that irrigated urban vegetation drives the biospheric signal we observe. Although 2015 was very dry, the biospheric seasonality we observe is similar to the 2006–2015 mean derived from an independent $\Delta^{14}C$ record in the Los Angeles area, indicating that 2015 biospheric exchange was not highly anomalous. The presence of a large and seasonally varying biospheric signal even in the relatively dry climate of Los Angeles implies that atmospheric estimates of fossil fuel–CO_2 emissions in other, potentially wetter, urban areas will be biased in the absence of reliable methods to separate fossil and biogenic CO_2.

radiocarbon | urban | carbon dioxide

Megacities, urban regions with populations >10 million, are global foci of both population and CO_2 emissions from combustion of fossil fuels. As of 2005, it is estimated that global CO_2 emissions from these cities were 1.1 Pg C y^{-1}, representing 12% of the global total (1). While just ∼6% of the global population now resides in ∼45 megacities, this population fraction is expected to increase throughout this century (2). As a result, global megacity emissions are forecast to reach 2.2 Pg C y^{-1} by 2050 (1), a total larger than current emissions for any single country except China. Thus, determining megacity emissions and their trends will be an important element of any effort to assess the efficacy of emission mitigation strategies (3), especially because subnational political entities such as cities and states or provinces are emerging as key players in anthropogenic emissions mitigation efforts (e.g., C40 Cities).

Fossil fuel–CO_2 emissions are typically determined using economic statistics describing fossil fuel use and associated emissions factors and can be estimated at a variety of scales ranging from whole countries to individual buildings (4). These data can also yield detailed information on emissions from fossil fuel use in different sectors, such as on-road transportation, residential heating, and power generation. However, such "bottom-up" inventories often take time to compile and update and frequently lack quantitative uncertainty estimates (e.g., ref. 5). In contrast, "top-down" approaches use distributed atmospheric measurements to estimate emissions. Although top-down studies tend to lack sectoral specificity, they implicitly include all possible sources within a geographic region. While top-down estimates may be subject to systematic errors in atmospheric transport (e.g., refs. 6, 7), interannual variability and trends of CO_2 fluxes are less likely to be impacted by systematic transport errors (8). Both bottom-up and top-down approaches have the potential to provide near real-time information to policy makers (9, 10) and, taken together, have the potential to provide complementary sectoral information and verifiable emissions totals.

A major challenge in top-down CO_2 emissions estimation is accurately partitioning fossil fuel and biospheric fluxes. Incorrect estimation of biospheric contributions can lead to equally

Significance

Megacities contribute significantly to national and global CO_2 emissions and are an increasingly important element of emissions mitigation efforts. Atmospheric monitoring helps to characterize urban emissions, but CO_2 measurements alone cannot distinguish between biogenic and fossil fuel contributions to observed CO_2 enhancements. We use measurements of CO_2 and the fossil fuel tracer $^{14}CO_2$ to demonstrate that even for highly urbanized and arid environments such as Los Angeles, the managed urban biosphere contributes significantly to the local carbon budget. These findings highlight the need to understand and quantify urban biospheric CO_2 in order to more accurately measure and track fossil fuel–CO_2 emissions and the impact of urban greening campaigns, as needed to evaluate and optimize emissions mitigation strategies.

Author contributions: J.B.M., S.J.L., C.E.M., and R.M.D. designed research; J.B.M., S.J.L., K.R.V., C.E.M, Y.V., and S.N. performed research; V.Y. contributed new reagents/analytic tools; J.B.M. and S.J.L. analyzed data, provided much of the radiocarbon data, and wrote the paper with contributions from all authors; K.R.V. contributed to sampling design, collected samples, and contributed data; S.N. collected samples and provided data; and C.D.S. contributed to sample collection.

The authors declare no competing interest.

This article is a PNAS Direct Submission. R.C.C. is a guest editor invited by the Editorial Board.

[1]To whom correspondence may be addressed. Email: John.B.Miller@noaa.gov.

[2]Present address: Arizona Institutes for Resilience, University of Arizona, Tucson, AZ 85712.

[3]Present address: Planning and Climate Protection Division, Bay Area Air Quality Management District, San Francisco, CA 94105.

[4]Present address: Whisker Labs, Germantown, MD 20876.

This article contains supporting information online at https://www.pnas.org/lookup/suppl/doi:10.1073/pnas.2005253117/-/DCSupplemental.

First published October 12, 2020.

erroneous fossil fuel–CO_2 quantification (6), and vice versa. At continental to global scales, fossil fuel–CO_2 emissions are typically assumed to be perfectly known from inventories with any residual CO_2 signal assigned to the biosphere, although some studies have relaxed this assumption (6, 11–13). On the other hand, at the urban scale, many top-down CO_2 studies have assumed zero biospheric influence (14–19) or adopted model-based estimates of biospheric fluxes and then used atmospheric CO_2 measurements to determine the balance attributable to emissions from fossil fuel combustion (20–22). Despite recent advances in modeling urban biospheric CO_2 fluxes (23), their magnitude and variability remain poorly known. Accurately quantifying urban biospheric fluxes and their seasonal variation is essential because any deviation of true and modeled (or assumed) biospheric fluxes would be translated into an observational bias in the magnitude and, possibly, the year-to-year trends of derived fossil fuel–CO_2 emissions.

For Los Angeles (L.A.), a megacity spread over more than 15,000 km^2 with a population of ~18 million (*SI Appendix*, Table S3), both bottom-up and top-down studies are adding to our understanding of its substantial urban CO_2 fluxes. The Hestia–L.A. data product (4) quantifies fossil fuel–CO_2 emissions for five counties in the L.A. region down to the level of roads and individual buildings. Total emissions are estimated to be ~45 Tg C y^{-1}, with the on-road (43%) and industrial (25%) sectors being the largest contributors. Atmospheric CO_2 monitoring as part of the Los Angeles Megacity Carbon Project (24) began in 2013 with the aim of estimating CO_2 emissions using a network of observation sites within and surrounding the megacity. However, Hestia–L.A. focuses exclusively on fossil fuel–CO_2 emissions, while L.A. megacity CO_2 measurements detect the total CO_2 flux (fossil plus biogenic). To date, there are also no available bottom-up models of urban biospheric CO_2 for the L.A. region. One previous study (25) simulated net biospheric CO_2 flux for the region, but assumed zero flux for the urban area. In general, simulating urban biospheric fluxes for L.A. is difficult, given the high spatial heterogeneity of the landscape combined with the paucity of urban flux measurements (e.g., chambers or eddy-flux towers) that would constrain model parameters relating to photosynthesis and respiration. Some previous studies focusing on fossil fuel–CO_2 in the L.A. area estimated biogenic CO_2 contributions, but they were either conducted over short periods (26) or used a single site of potentially limited representativity (27). CO_2 fluxes have also been calculated for L.A. using data from aircraft measurement campaigns (28) and remote sensing (18), but these studies made no attempt to account for biogenic contributions. Despite these studies, little is currently known about CO_2 fluxes from the urban biosphere in the L.A. megacity.

In this study, we interpret measurements of CO_2 mole fraction and their ^{14}C:C ratios (expressed as $\Delta^{14}C$) obtained from air samples collected two to three times per week over more than a year at three sites within the Los Angeles Megacity Carbon Project greenhouse gas network (24) (Fig. 1). $\Delta^{14}C$ is a nearly unambiguous tracer for fossil fuel–CO_2 because, unlike all other CO_2 sources to the atmosphere, fossil fuel-derived CO_2 contains no ^{14}C (e.g., refs. 29, 30). Past urban studies have used measurements of CO_2 and $\Delta^{14}C$ to estimate the contribution of fossil fuel combustion to observed CO_2 variation (e.g., refs. 27, 31–35), but here we focus on using atmospheric measurements to better understand the timing and origin of urban biospheric fluxes in the L.A. megacity. In contrast to inventories, models, or remote sensing observations, our data offer relatively direct measures of urban biospheric and fossil CO_2 fluxes. Our results show an unequivocal CO_2 signal originating from the urban biosphere, despite the density of the urban development and the naturally dry Mediterranean environment. Additionally, our $\Delta^{14}C$ measurements show that CO_2 fluxes from the L.A. urban biosphere vary seasonally, with a timing best explained by managed urban water use rather than precipitation. While our observations took place in a year of extreme drought, we suggest that the influence of managed water use on the urban biosphere may be a persistent feature of the associated CO_2 uptake response, occurring even in years when drought was less severe or absent.

Methods

From November 2014 to March 2016, we used National Oceanic and Atmospheric Administration (NOAA) programmable flask packages (PFPs) and programmable compressor packages (36) to collect paired air samples at 2 PM local standard time at three existing Los Angeles Megacity Carbon Project sites: the corners of building rooftops at the University of Southern California (USC) and California State University, Fullerton (FUL) at 50 m above ground level, and from a 51-m tower in Granada Hills (GRA) (Verhulst, 2017 (24), *SI Appendix*). These sites were chosen to represent a broad swath of the most densely populated part of the L.A. Basin. We measured the CO_2 mole fraction on one member of PFP sample pairs returned to the NOAA Global Monitoring Laboratory. After measurement of other greenhouse gases on NOAA's high-precision/high-accuracy greenhouse gas measurement system (36), we extracted residual air from PFP flask pairs and isolated CO_2 for later ^{14}C measurement using established cryogenic techniques (37). We then graphitized pure CO_2 samples and sent them to the University of California, Irvine, Keck Accelerator Mass Spectrometry Facility for high-precision $\Delta^{14}C$ measurement. We specify a one-sigma measurement uncertainty of ~1.8‰ based on repeat measurement of control samples (38), equivalent to ~1.2 parts per million (ppm) of recently added fossil fuel–CO_2 (*SI Appendix*). All CO_2 and $\Delta^{14}C$ data are provided in Dataset S1. We

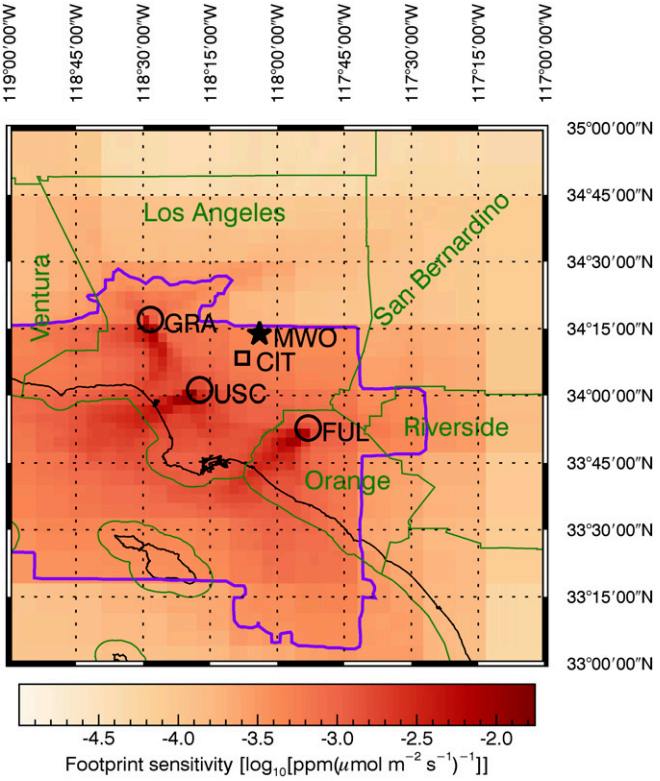

Fig. 1. Annual average footprint (surface flux sensitivity) for the three Los Angeles Megacity Carbon Project sampling sites used in this study (open circles). Green lines represent county boundaries. The purple line represents the 50% influence contour (50% of the total footprint influence is inside the contour). The full domain of the footprints (which go back 60 h) is from 121°W–114°W and 31.4°N–36.8°N and includes substantial portions of desert and ocean. Also note that the WRF-STILT footprint model decreases its resolution away from the sampling sites, as can be seen in the block-like nature of the footprints and contours. The star represents the high-altitude background site (MWO), and the square shows the location of Newman et al. (2016) Pasadena (CIT) samples discussed in the text (27).

calculated average surface sensitivities for all samples during the study period using 1.33-km resolution Weather Research and Forecasting model (WRF) meteorology (version 3.6.1) in conjunction with the Stochastic Time-Inverted Lagrangian Transport (STILT) back-trajectory model to create individual sample "footprints" with 0.03° × 0.03° resolution (39). The average footprints show that our midafternoon samples are sensitive to fluxes from large portions of the L.A. Basin, especially L.A. County (Fig. 1).

To quantify CO_2 enhancements for L.A., we define representative background CO_2 and $\Delta^{14}C$ levels based on nighttime (2 AM local standard time) measurements made at Mount Wilson Observatory (MWO, 1,670 m above sea level (m.a.s.l.); Fig. 1), when polluted L.A. Basin boundary layer air has typically descended, and the site samples the relatively clean, well-mixed free troposphere. Data quality control additionally excluded a few obvious low $\Delta^{14}C$ outliers, corresponding to air with high fossil fuel–CO_2. A total of 367 paired $\Delta^{14}C$ and CO_2 measurements at GRA ($n = 115$), USC ($n = 125$), and FUL ($n = 127$) were also filtered to maximize the representativeness of the data. First, all samples associated with windspeeds less than 1.5 m s^{-1} were excluded from further analysis to avoid stagnant conditions (*SI Appendix*); second, in the case of USC and FUL, samples with wind directions corresponding to the building roof were excluded to minimize the possibility of contamination from rooftop exhaust vents, leaving 271 paired measurements for use in the remainder of the analysis. Individual CO_2 and $\Delta^{14}C$ background values were created by fitting curves to the screened MWO data to permit resampling at the times of observations at GRA, USC, and FUL (Fig. 2). Other L.A.-area locations, such as San Clemente Island, may provide better representation of background air at certain times of year (24), but MWO is the only local background site with a high density of $\Delta^{14}C$ measurements. Moreover, carbon monoxide (CO) measurements of the same nighttime MWO air samples used to construct the $\Delta^{14}C$ background are similar to the Pacific marine boundary layer CO reference (40) at 33°N (*SI Appendix*, Fig. S1). This suggests that nighttime MWO measurements should provide a reliable representation of relatively clean background air coming from either on or off shore into the L.A. Basin. A previous fossil fuel–CO_2 study using $\Delta^{14}C$ data from Pasadena (CIT) in the eastern part of the L.A. Basin (27) used Utqiagvik, AK (BRW) $\Delta^{14}C$ data as a background, because measurements from nearby sites were not available. MWO should provide for improved representation of the local $\Delta^{14}C$ background, given its proximity to the L.A. greenhouse gas monitoring sites and the similarity to offshore records of CO.

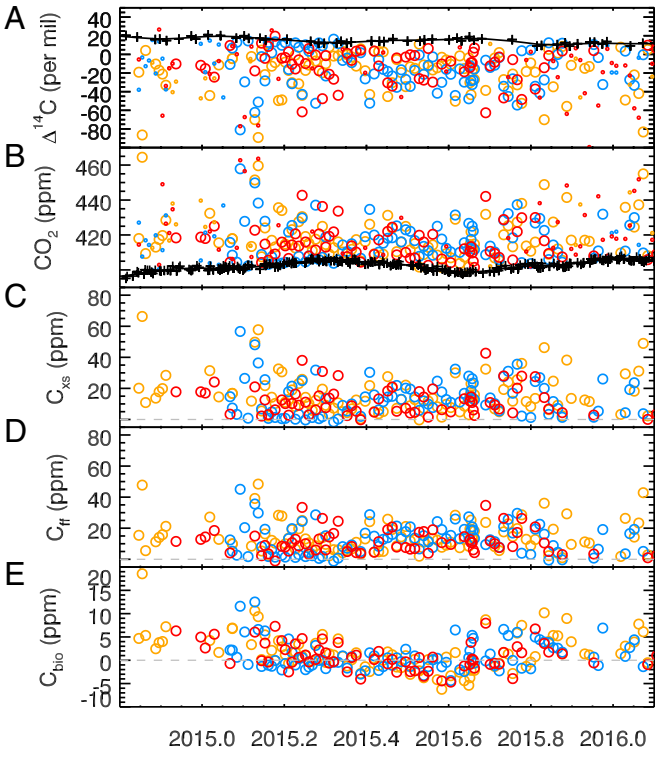

Fig. 2. Time series of measured (*A* and *B*) and derived (*C*–*E*) quantities from three different sampling sites, as described in the main text. Orange is USC; Blue is GRA; Red is FUL. Black line and crosses are the MWO (background) smooth curve and data, respectively. Small symbols in *A* and *B* represent data with windspeeds less than 1.5 m s^{-1} or wind directions from over building rooftops.

Results and Discussion

Fig. 2 *A* and *B* show $\Delta^{14}C$ and CO_2 measurements for GRA, USC, and FUL in addition to background values and curve fits from MWO. Over the course of the study period, CO_2 at the three sites was enhanced relative to background by 14.6 ± 11.8 ppm (multisite mean and one-sigma SD). Mean $\Delta^{14}C$ was depleted by −30.9 ± 21.4‰ relative to background, reflecting the substantial influence of ^{14}C-free CO_2 emissions from fossil fuel combustion. To better understand the relationship between CO_2 enhancements and $\Delta^{14}C$ depletions, we first performed an isotopic mixing analysis (41) using data from all three sites (Fig. 3). We start from mass balance equations for CO_2 and its isotopic composition (Eqs. **1** and **2**) (30), where CO_2 mole fractions and $\Delta^{14}C$ values are abbreviated as C and Δ; "obs" are GRA, USC, and FUL observations of either C or Δ; "bg" is the interpolated MWO background; "ff," "r," and "p" represent the fossil fuel, respiratory, and photosynthetic mole fraction contributions modifying the background; and "xs" represents the sum of all such contributions above or below background.

$$C_{obs} = C_{bg} + C_{ff} + C_r + C_p = C_{bg} + C_{xs} \quad [1]$$

$$\Delta_{obs}C_{obs} = \Delta_{bg}C_{bg} + \Delta_{ff}C_{ff} + \Delta_rC_r + \Delta_pC_p = \Delta_{bg}C_{bg} + (\Delta \times C)_{xs} \quad [2]$$

In order to provide a first-order estimate of the average biogenic and fossil CO_2 contributions to C_{xs}, we regress C_{xs} vs. $(\Delta \times C)_{xs}$, where the slope, Δ_{source}, is the flux-weighted average isotopic signature of the biogenic and fossil fractions (Fig. 3). As expected from visual inspection of Fig. 2 *A* and *B*, we retrieve a very high coefficient of determination, R^2, between C_{xs} and $(\Delta \times C)_{xs}$ of 0.94. However, the slope, Δ_{source}, is −783 ± 11‰. If C_{xs} were due solely to fossil fuel emissions, then Δ_{source} would equal −1,000‰ because fossil fuel contains zero ^{14}C. To determine the fossil and biogenic fractions of C_{xs}, f_{ff} and f_{bio} (corresponding to C_{ff} and $C_{bio,}$ where $C_{bio} = C_r + C_p$), we conduct a two end-member mixing analysis. Δ_{ff} = −1,000‰ and Δ_{bio} = −16.5‰ under the assumption that Δ_{bio} is in equilibrium with the observed local atmosphere, Δ_{obs}. This leads to estimated biogenic and fossil fractions of C_{xs} for L.A. of ∼20% and ∼80% (*SI Appendix*). Site-specific values of Δ_{source} for GRA, USC, and FUL are −786 ± 18‰, −758 ± 19‰, and −787 ± 30‰, respectively, and overlap the slope from the combined dataset within uncertainties. Similarity between these sites was also observed previously in the statistical distributions of quasi-continuous measurements of CO_2 mole fraction (24) and justifies pooling the data for the remainder of the analysis.

In order to isolate C_{ff} on a sample-by-sample basis, as in previous work (30), we set $\Delta_p = \Delta_{bg}$ and combine Eqs. **1** and **2** (Fig. 2*D*):

$$C_{ff} = C_{obs}(\Delta_{obs} - \Delta_{bg})/(\Delta_{ff} - \Delta_{bg}) - C_r(\Delta_r - \Delta_{bg})/(\Delta_{ff} - \Delta_{bg}) \quad [3]$$

Eq. **3** shows that C_{ff} depends not just on the measured quantities, but also weakly on the biospheric disequilibrium term, $-C_r(\Delta_r - \Delta_{bg})/(\Delta_{ff} - \Delta_{bg})$ (30, 43). To represent a likely maximum effect, we assume an isotopic disequilibrium $(\Delta_r - \Delta_{bg})$ of +50‰ (corresponding to an atmospheric growth rate of −5‰ y^{-1} and a biospheric residence time of 10 y) and a value of C_r of 5 ppm, which is about 25% larger than the mean winter (November–February) net biosphere mole fraction, C_{bio}, that is likely

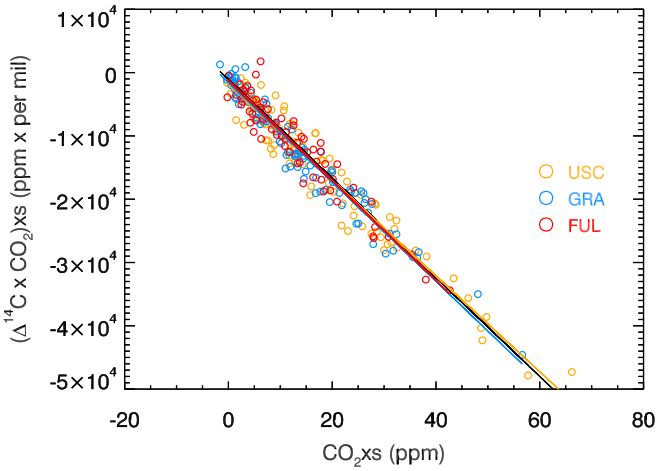

Fig. 3. Isotope mixing analysis. The slopes of the fitted lines are isotope signatures of the flux-weighted sources, calculated as described in the main text. Colored lines represent the fits to data from each site, and the black line represents the fit to data from all sites. The slope of the black line is −783 ± 11‰ indicating a substantial contribution of biogenic sources to observed CO_2 variability, as discussed in the text. Only data passing wind-speed and direction filtering criteria are shown and used in the regression. Linear regressions are calculated following the method of York et al. (2004) as described in *SI Appendix* (42).

dominated by C_r. This results in a disequilibrium correction of +0.25 ± 0.00 ppm (one-sigma SD), but the presence of the disequilibrium term has no impact on our conclusions. Derived C_{ff} averages 13.2 ± 9.4 ppm with minimum and maximum values of −1.3 and 48.4 ppm. (Note that a few instances of negative, nonphysical, C_{ff} are expected, given the one-sigma uncertainty of 1.2 ppm.) Although mean C_{ff} during the winter months (November–February; 14.0 ± 12.7 ppm) is nearly the same as during the summer (May–September; 13.2 ± 6.9 ppm), the variability is approximately twice as large in winter, mainly as a result of more instances of high C_{ff}. These likely result from increased atmospheric trapping of emissions in the boundary layer, as opposed to high emissions, because Hestia–L.A. (4) indicates that wintertime emissions are only 3% higher than those in summer. The fact that the annual SD of C_{ff} across all sites is 9.4 ppm, or 71% of its mean level, also suggests that atmospheric transport, rather than emissions, dominates the variability of observed C_{ff}. Such high variability in emissions is unlikely; large variations in atmospheric trapping of emissions due to variations in wind speed and planetary boundary layer (PBL) height are more likely.

C_{bio} (Fig. 2*E*) is calculated as the difference between C_{ff} and C_{xs} (Eq. **1**). It shows an annual mean value of 1.5 ± 1.9 ppm (mean and SD of monthly means), a mean wintertime enhancement of 3.5 ± 0.9 ppm, and a much smaller summertime mean enhancement of −0.3 ± 1.0 ppm. Fifty-six percent of all summertime C_{bio} values are negative, indicating some degree of net CO_2 uptake. In order to isolate the signal coming from the terrestrial biosphere, we estimate contributions to C_{bio} from biogenic sources such as biofuels and human respiration. According to the State of California's Air Resources Board (CARB) emissions inventory, ethanol and biodiesel in the "on-road" sector are a leading source of biofuel emissions in the inventory (3.1 Tg C y^{-1} statewide, or about 7% of total on-road), but other sectors such as "industrial" and "electricity production" (3.5 and 2.0 Tg C y^{-1}, or 17% and 15%, respectively) also include significant biofuel use. For all CO_2 emission sectors, we calculate biogenic:fossil emission ratios at the state level (where CARB inventory data are available) and apply these ratios to the same emission sectors for the five Southern California counties covered by the Hestia–L.A. emissions inventory (*SI Appendix*, Table S2). Considering all sectors, we find a ratio of biogenic to fossil fluxes of 0.103. We estimate emissions for human respiration and excretion by applying a global relationship between human population and total human metabolic emissions (44) to populations for the five counties in Hestia–L.A. We find a ratio of human metabolic to fossil fluxes of 0.057 (*SI Appendix*, Table S3). Thus, the overall biogenic:fossil emission ratio for human metabolism and use of biofuels, R_{bio}, is 0.160. Applying this combined factor, we isolate the C_{bio} contributions coming from urban ecosystems, which we define as $C_{bio}' = C_{bio} - R_{bio} \times C_{ff}$. This results in an average annual C_{bio}' enhancement of −0.6 ± 1.8 and wintertime and summertime C_{bio}' mean values of 1.5 ± 0.9 ppm and −2.3 ± 1.0 ppm, respectively. On average, individual C_{bio}' values are 2.1 ppm lower than C_{bio}. We test the sensitivity of C_{bio}' to the fuel-related portion of the overall correction factor by using an alternative biogenic:fossil ratio for fuel-related sectors of 0.050 derived from the Anthropogenic Carbon Emissions System version 2 (ACES v2) (45) (*SI Appendix*), resulting in an alternative R_{bio} of 0.107. The annual mean (based on monthly means) of C_{bio}' increases by 0.7 ppm, but the amplitude of the C_{bio}' seasonal cycle (November–January minus June–August; *SI Appendix*) remains unchanged at 4.3 ppm (*SI Appendix*, Fig. S2). This is not surprising, given that the correction factors are annual and that there is no significant seasonality in C_{ff}. Even in the case of uncorrected C_{bio}, the derived seasonal amplitude of 4.1 ppm is within 5% of the amplitude of the two C_{bio}' estimates. We also tested the sensitivity of the seasonal cycle amplitude of C_{bio}' to our choice of background site by using CO_2 and $\Delta^{14}C$ measurements from Niwot Ridge, CO (NWR), which lies ∼1,300 km northwest of MWO and 1,800 m higher in elevation. Despite substantially different seasonal cycles of CO_2 and $\Delta^{14}C$ at NWR and MWO (*SI Appendix*, Fig. S3), two thirds of the derived C_{bio}' amplitude is retained when using NWR as background. The relatively small sensitivity to rather different background values occurs because the local CO_2 and $\Delta^{14}C$ signals at GRA, USC, and FUL are so large.

The Mediterranean climate of Southern California is characterized by a winter rainy season that generally leads to a March/April maximum in carbon uptake for most unmanaged ecosystems (*SI Appendix*, Fig. S4). In contrast, the seasonality of derived C_{bio}' for the L.A. urban area resembles that of a temperate midlatitude ecosystem with maximum carbon uptake in the middle of the year (Fig. 4). In order to evaluate the possible impact of different moisture inputs on C_{bio}', we compare the timing of C_{bio}' to locally representative records of precipitation and urban water use (Fig. 4). The precipitation maximum occurs in winter, as expected, but is associated with net biospheric emission rather than the uptake response characterizing most unmanaged ecosystems in the region (*SI Appendix*, Fig. S4). On the other hand, the timings of observed C_{bio}' and urban water use are well correlated (Fig. 4 and *SI Appendix*, Fig. S5), with peak water use and CO_2 uptake in the summer months. This suggests that irrigation of urban turf (including lawns, golf courses, and parks) and other vegetation exerts a substantial control on urban C_{bio}', overwhelming the influence of local precipitation. Although water use totals include consumption from industrial use, indoor use, and outdoor landscape irrigation, seasonal variation of total usage is most likely dominated by landscape irrigation (46). The potential contribution of urban vegetation to C_{bio}' is also supported by high-resolution land surface classification for the L.A. area based on the Airborne Visible InfraRed Imaging Spectrometer (AVIRIS) (47) showing a footprint weighted-mean tree and turf cover of 14% in the upwind fetch of our measurement sites (*SI Appendix*, Fig. S6). Analysis of remote sensing and aerial photography also indicate tree coverage of 21% and irrigated lawn coverage of 12% for the city of L.A. (48). Of the

available records of net ecosystem exchange (NEE) from unmanaged ecosystems, only that for the high-altitude (1,770 m.a.s.l.) Oak/Pine forest exhibits a seasonal cycle that is roughly in phase with the L.A. C_{bio}' signal (*SI Appendix*, Fig. S4). While the San Gabriel mountains that form the northern border of the L.A. Basin contain similar ecosystems, they are likely too distant from our sites to contribute significantly to observed C_{bio}'. Assuming that monthly mean NEE for the Oak/Pine site represents the NEE for all local forest cover above 1,500 m.a.s.l., we convolve sample footprints at each site with NEE maps and find the resulting simulated C_{bio}' amplitude at our measurement sites is not more than ~0.3 ppm (*SI Appendix*, Fig. S7). Ultimately, sources such as urban trees and turf must be responsible for the vast majority of the observed C_{bio}' signal because unlike CO_2 sources such as biofuel combustion and human metabolism, which can only be emissive, our observations also require seasonal carbon sinks.

As noted earlier, the L.A. region (located within the "South Coast District" of California) experienced "extreme drought" during our study period, with Palmer Drought Severity Index (PDSI) levels below −4 in 2015 (*SI Appendix*, Fig. S8). The drought can also be seen in the deviation of local precipitation in 2015 from the 2014–2019 average and range (Fig. 4); in 2015, less than 60 mm of rain fell during the January through March rainy season. In order to assess the impact of the 2015 drought conditions on C_{bio}', we analyze the CIT $\Delta^{14}C$ record of Newman and coauthors (27), which has been extended to encompass 2006–2015, overlapping the period of our observations. The record consists of approximately twice-monthly $\Delta^{14}C$ measurements made on air samples collected at about 10 m above ground level on the campus of the California Institute of Technology, located in the city of Pasadena in the eastern L.A. Basin. Following Newman et al. (27), we calculate C_{bio} using BRW for $\Delta^{14}C$ background and Scripps Pier measurements at La Jolla, California (LJO) for CO_2 background; to estimate C_{bio}' we use the default value of R_{bio} derived above. The CIT 2006–2015 mean seasonal cycle (Fig. 4 and *SI Appendix*, Fig. S9) is broadly similar to the 2015 seasonal cycle of C_{bio}' obtained from the L.A. megacity site data, except that the mean CIT results show maximum uptake in June rather than July. In 2015, CIT exhibits a C_{bio}' minimum in May. For 2015, the only full year for which MWO $\Delta^{14}C$ data are currently available, we can recalculate CIT C_{bio}' using the nearer MWO site as background for CO_2 and $\Delta^{14}C$ instead of LJO and BRW, respectively. This results in a 2015 CIT C_{bio}' minimum in July, with a seasonality very similar to C_{bio}' of the L.A. megacity sites (*SI Appendix*, Fig. S10). This suggests that the timing of the 2006–2015 mean CIT C_{bio}' minimum could in fact be slightly later in the year, more in line with our 2015 observations. Irrespective of potential background artifacts, what is most notable about the 2006–2015 record of C_{bio}' at CIT is that 2015 does not stand out from the other 10 y (*SI Appendix*, Fig. S9). Although there were very dry (7 y with PDSI < −3) and less dry (3 y with PDSI > −3) years between 2006 and 2015, the difference in average C_{bio}' seasonal cycles between the two regimes is relatively small (*SI Appendix*, Fig. S9). The mean month of the C_{bio}' minimum for years with PDSI < −3, PDSI > −3, and the 10-y mean all occur in June, and the mean amplitudes (7.7 ± 3.1 ppm for dry years and 5.2 ± 1.0 ppm for "wet" years) are not statistically different ($P > 0.10$). Neglecting the possibility that the CIT minima may be biased early due to misrepresentation of background, estimated maximum CO_2 uptake signals are still much closer to peak water usage in July and August than to the period of peak climatological rainfall in January and February. This suggests that the influence of anthropogenic water inputs on urban biospheric CO_2 exchange in L.A. is pervasive and not restricted to occasions of extreme drought such as occurred during our study period. Furthermore, while the 2015 L.A. megacity observations were associated with extreme drought, such conditions may increasingly represent the "new normal." Between 2000 and 2019, 10 y have been "severe" (−4 < PDSI < −3) or "extreme" droughts in the South Coast District (*SI Appendix*, Fig. S8).

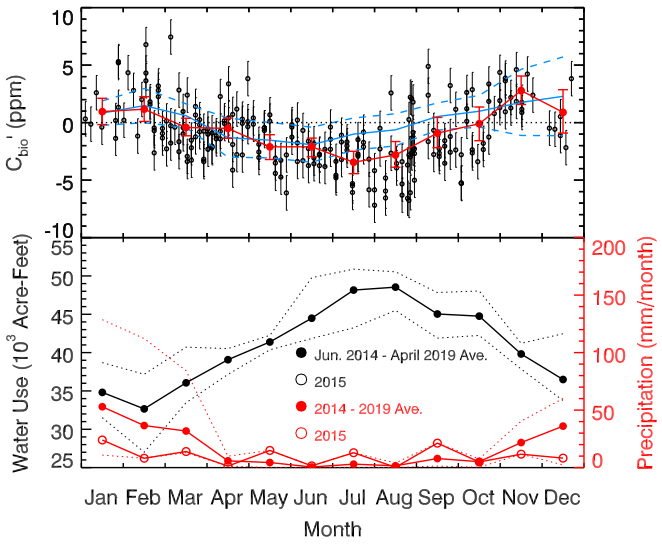

Fig. 4. (*Top*) The urban biospheric fraction of the excess CO_2 signal (C_{bio}') shown for all samples (passing windspeed and wind direction screening) as open black circles with one-sigma random errors. Monthly mean C_{bio}' values are overplotted as filled red symbols. Red error bars represent 95% confidence intervals (CIs) for the means, calculated using a bootstrap method, as described in *SI Appendix*. The solid blue line shows the 2006–2015 mean monthly C_{bio}' from CIT (using LJO and BRW as background for CO_2 and $\Delta^{14}C$, respectively), with the 10-y SDs shown in dashes. (*Bottom*) Water inputs to the study domain. Black symbols and lines represent total water usage for the area served by the L.A. Department of Water and Power as reported to the State of California Water Board (https://www.waterboards.ca.gov/water_issues/programs/conservation_portal/conservation_reporting.html, accessed June 2019). Red symbols and lines represent monthly total precipitation from the Global Precipitation Climatology Project (GPCP v1.3) for the 1° × 1° degree grid cell containing the city of L.A. Red and black dashed lines represent the upper and lower bounds for the date ranges in the legend of either city water usage or precipitation and are referenced to the respective solid line with solid symbols. The lines with open symbols represent water usage or precipitation for 2015.

Finally, we consider the observational bias in fossil fuel–CO_2 that would arise throughout the year by neglecting the role of biogenic CO_2 and assuming that all of the CO_2 enhancement observed in L.A. is derived from fossil fuel use. We show this effect in Fig. 5 by plotting the monthly relative bias, $C_{xs}/C_{ff} - 1$. For winter months (November–February) when C_{bio} is positive, the mean error is +27%, and during summer (May–September), when C_{bio} tends to be negative, the bias is −7%. The maximum and minimum monthly mean biases are +56 ± 12% (68% CI) and −21 ± 8%, occurring in November and July, respectively. These biases would not be detected without reliable methods to separate C_{bio} and C_{ff} (such as $^{14}CO_2$ measurements), whether from surface measurements or remote sensing of the total atmospheric column. We note that relative bias ($C_{xs}/C_{ff} - 1$) will be the same for observations of the total atmospheric column as for the PBL, if C_{ff} and C_{bio} are zero above the top of the PBL. This condition will be close to true when air parcels above the top of the PBL have minimal surface influence.

Conclusions

We have shown the combination of atmospheric CO_2 and $\Delta^{14}C$ data in the L.A. megacity to be a powerful tracer for both the fossil and biogenic components of the total urban CO_2 signal.

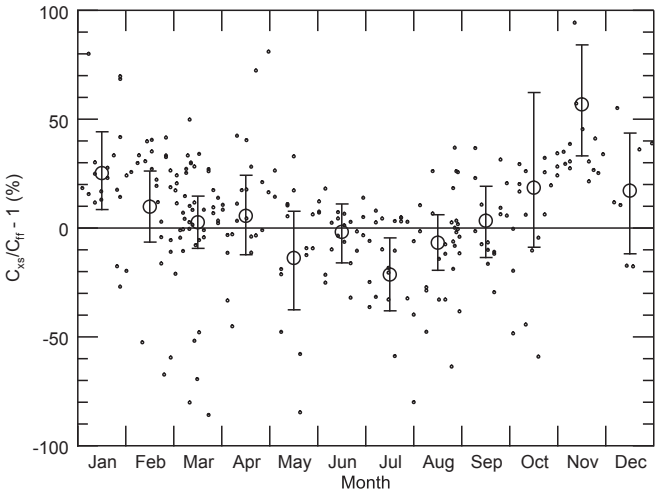

Fig. 5. Relative error induced by assuming that all of the C_{xs} signal is fossil (i.e., $C_{bio} = 0$). Small circles are values of $C_{xs}/C_{ff} - 1$ for individual samples (passing the windspeed and wind direction threshold). Large circles are monthly means of those values; error bars are 95% CIs for medians calculated using bootstrap, with replacement, of individual values within a month, further accounting for individual uncertainties on $C_{ff}/C_{xs} - 1$ values (as described in *SI Appendix*).

Overall, we find that ∼20% of local L.A. CO_2 variability is biogenic. Our analysis further reveals that the amplitude of CO_2 originating from the urban biosphere (4.3 ppm) is 33% of the annual mean fossil fuel contribution (13.0 ppm), a surprisingly large fraction for a naturally dry metropolitan area seemingly dominated by transportation and industrial emissions. The seasonality of observation-based C_{bio}' from the drought year of 2015 is consistent with controls on urban NEE from urban water usage, and there is further evidence from the 10-y CIT C_{bio}' record that urban water usage, more than rainfall, may drive the urban NEE response even in years when drought is less severe or absent. In the L.A. megacity, human activity appears to influence both fossil and vegetation CO_2 fluxes—i.e., even the biospheric fluxes we observe are anthropogenic.

Accurately measuring the biospheric contribution to urban CO_2 in L.A., and possibly other naturally arid urban areas in the United States and throughout the world, will be important in avoiding biases in estimated fossil fuel CO_2 emissions that would otherwise result from measuring CO_2 alone. The ability to separately track biogenic and fossil carbon fluxes will also become increasingly important to assess the impact of policies such as L.A.'s "Million Trees L.A." initiative (48) and to improve our understanding of the relationship between urban biospheric CO_2 fluxes and natural and anthropogenic water inputs in the presence of a changing climate. Many current and future megacities with extensive tree cover are wetter than L.A. For tropical and subtropical megacities such as Mumbai, India, and São Paulo, Brazil, this may result in annual average and monthly biospheric CO_2 signals larger than we observe in this study. In the absence of constraints from reliable fossil fuel–CO_2 tracers such as $\Delta^{14}C$, undetected biospheric signals would result in potentially significant observational biases in fossil fuel–CO_2 emissions that could vary from year to year, hampering the ability to accurately quantify urban fossil fuel–CO_2 emissions trends using top-down methods. $\Delta^{14}C$ and CO_2 measurements from a variety of temperate midlatitude cities such as Indianapolis, Heidelberg, Paris, and Krakow (29, 31, 34, 49) also show that, even during winter, neglecting C_{bio} may result in biased estimates of atmospheric concentrations and emissions of fossil fuel–CO_2.

It may not be feasible to deploy $\Delta^{14}C$ measurements in all large cities to the extent we have in L.A. and other urban areas such as Indianapolis (34). However, periodic $\Delta^{14}C$ measurements will be necessary to track the interannual variability and trends of C_{ff} and C_{bio} resulting from growing urban populations, changing fuel types and usage, emissions reduction efforts, and urban greening campaigns, as well as climate. One effective monitoring strategy that greatly leverages relatively costly ^{14}C measurements may be to "calibrate" other anthropogenic tracers such as CO against ^{14}C-based C_{ff} (33, 35). Since CO can be measured continuously and at lower cost than ^{14}C, it can be used together with a limited number of ^{14}C measurements to provide an accurate and quasi-continuous proxy for C_{ff}. Because constraining C_{ff} also constrains C_{bio}, such an observing strategy could be used to evaluate and improve models of the urban biosphere, such as the Urban Vegetation Photosynthesis and Respiration Model (VPRM) (23). Measurements of CO_2, $\Delta^{14}C$, and CO (or other proxies) have great potential to optimize both fossil and biospheric fluxes using urban-scale inversions and can thus improve the accuracy of both top-down and bottom-up approaches meant to assess the efficacy of urban emissions mitigation efforts.

Data Availability. All study data are included in the article and *SI Appendix*.

ACKNOWLEDGMENTS. We thank Jack Higgs, Jon Kofler, Arlyn Andrews, Eric Moglia, Patricia Lang, and Ed Dlugokencky for assistance with sampling technology, logistics, and CO_2 measurements. Chad Wolak, Stephen Morgan, and Patrick Cappa prepared samples for $\Delta^{14}C$ measurement; John Southon made the $\Delta^{14}C$ measurements. We thank Ray Weiss, Ralph Keeling, and Jooil Kim for accommodating air sampling at three Los Angeles Megacity Carbon Project sites and the University of Southern California and California State University, Fullerton, for hosting two of those sites. We thank Bill Angel and Earth Networks for Megacities Carbon Project site support. We also thank Connor Gately for providing ACES v2. This work was supported in part by a grant to J.B.M. and S.J.L. (NOAA Award NA14OAR4310177). A portion of this research was carried out at the Jet Propulsion Laboratory, California Institute of Technology, under a contract with the National Aeronautics and Space Administration (80NM0018D0004) including support from Carbon Cycle and Ecosystems project 13-CARBON13_2-0074 and the Earth Science Division's OCO-2 program. The broader Los Angeles Megacity Carbon Project is supported by NASA, the National Institute for Standards and Technology, and the California Air Resources Board.

1. G. A. Folberth, T. M. Butler, W. J. Collins, S. T. Rumbold, Megacities and climate change—A brief overview. *Environ. Pollut.* **203**, 235–242 (2015).
2. United Nations, *World Urbanization Prospects: The 2018 Revision (ST/ESA/SER.A/420)*, Population Division of the Department of Economic and Social Affairs, Ed. (United Nations, New York, 2019).
3. R. M. Duren, C. E. Miller, Measuring the carbon emissions of megacities. *Nat. Clim. Change* **2**, 560–562 (2012).
4. K. R. Gurney *et al.*, The Hestia fossil fuel CO_2 emissions data product for the Los Angeles megacity (Hestia-LA). *Earth Syst. Sci. Data* **11**, 1309–1335 (2019).
5. G. Janssens-Maenhout *et al.*, *Fossil CO_2 and GHG Emissions of all World Countries*, (Publications Office of the European Union, Luxembourg, 2017).
6. S. Basu, J. B. Miller, S. Lehman, Separation of biospheric and fossil fuel fluxes of CO_2 by atmospheric inversion of CO_2 and $^{14}CO_2$ measurements: Observation System Simulations. *Atmos. Chem. Phys.* **16**, 5665–5683 (2016).
7. S. Feng *et al.*, Los Angeles megacity: A high-resolution land–atmosphere modelling system for urban CO_2 emissions. *Atmos. Chem. Phys.* **16**, 9019–9045 (2016).
8. D. F. Baker *et al.*, TransCom 3 inversion intercomparison: Impact of transport model errors on the interannual variability of regional CO_2 fluxes, 1988-2003. *Global Biogeochem. Cycles* **20**, GB1002 (2006).
9. C. Le Quéré *et al.*, Temporary reduction in daily global CO_2 emissions during the COVID-19 forced confinement. *Nat. Clim. Change* **10**, 647–653 (2020).
10. R. M. Duren *et al.*, California's methane super-emitters. *Nature* **575**, 180–184 (2019).
11. K. R. Gurney *et al.*, Sensitivity of atmospheric CO_2 inversions to seasonal and interannual variations in fossil fuel emissions. *J. Geophys. Res.* **110**, D10308 (2005).
12. Y. P. Shiga, A. M. Michalak, S. M. Gourdji, K. L. Mueller, V. Yadav, Detecting fossil fuel emissions patterns from subcontinental regions using North American in situ CO_2 measurements. *Geophys. Res. Lett.* **41**, 4381–4388 (2014).
13. S. Basu *et al.*, Estimating US fossil fuel CO_2 emissions from measurements of 14C in atmospheric CO_2. *Proc. Natl. Acad. Sci. U.S.A.* **117**, 13300–13307 (2020).
14. E. A. Kort, C. Frankenberg, C. E. Miller, T. Oda, Space-based observations of megacity carbon dioxide. *Geophys. Res. Lett.* **39**, L17806 (2012).

15. J. Hakkarainen, I. Ialongo, J. Tamminen, Direct space-based observations of anthropogenic CO_2 emission areas from OCO-2. *Geophys. Res. Lett.* **43**, 11400–11406 (2016).
16. D. Wunch, P. O. Wennberg, G. C. Toon, G. Keppel-Aleks, Y. G. Yavin, Emissions of greenhouse gases from a North American megacity. *Geophys. Res. Lett.* **36**, L15810 (2009).
17. T. Lauvaux *et al*., High-resolution atmospheric inversion of urban CO_2 emissions during the dormant season of the Indianapolis Flux Experiment (INFLUX). *J. Geophys. Res. Atmos.* **121**, 5213–5236 (2016).
18. J. K. Hedelius *et al*., Southern California megacity CO_2, CH_4, and CO flux estimates using ground- and space-based remote sensing and a Lagrangian model. *Atmos. Chem. Phys.* **18**, 16271–16291 (2018).
19. D. Wu, J. C. Lin, T. Oda, E. A. Kort, Space-based quantification of per capita CO_2 emissions from cities. *Environ. Res. Lett.* **15**, 035004 (2020).
20. K. McKain *et al*., Assessment of ground-based atmospheric observations for verification of greenhouse gas emissions from an urban region. *Proc. Natl. Acad. Sci. U.S.A.* **109**, 8423–8428 (2012).
21. J. Staufer *et al*., The first 1-year-long estimate of the Paris region fossil fuel CO_2 emissions based on atmospheric inversion. *Atmos. Chem. Phys.* **16**, 14703–14726 (2016).
22. M. Sargent *et al*., Anthropogenic and biogenic CO_2 fluxes in the Boston urban region. *Proc. Natl. Acad. Sci. U.S.A.* **115**, 7491–7496 (2018).
23. B. S. Hardiman *et al*., Accounting for urban biogenic fluxes in regional carbon budgets. *Sci. Total Environ.* **592**, 366–372 (2017).
24. K. R. Verhulst *et al*., Carbon dioxide and methane measurements from the Los Angeles Megacity Carbon Project—Part 1: Calibration, urban enhancements, and uncertainty estimates. *Atmos. Chem. Phys.* **17**, 8313–8341 (2017).
25. C. Park *et al*., CO_2 transport, variability, and budget over the Southern California Air Basin using the high-resolution WRF-VPRM model during the CalNex 2010 campaign. *J. Appl. Meteorol. Climatol.* **57**, 1337–1352 (2018).
26. S. Newman *et al*., Diurnal tracking of anthropogenic CO_2 emissions in the Los Angeles Basin megacity during spring 2010. *Atmos. Chem. Phys.* **13**, 4359–4372 (2013).
27. S. Newman *et al*., Toward consistency between trends in bottom-up CO_2 emissions and top-down atmospheric measurements in the Los Angeles megacity. *Atmos. Chem. Phys.* **16**, 3843–3863 (2016).
28. J. Brioude *et al*., Top-down estimate of surface flux in the Los Angeles Basin using a mesoscale inverse modeling technique: Assessing anthropogenic emissions of CO, NO_x and CO_2 and their impacts. *Atmos. Chem. Phys.* **13**, 3661–3677 (2013).
29. I. Levin, B. Kromer, M. Schmidt, H. Sartorius, A novel approach for independent budgeting of fossil fuel CO_2 over Europe by $^{14}CO_2$ observations. *Geophys. Res. Lett.* **30**, 2194 (2003).
30. J. C. Turnbull *et al*., Comparison of $^{14}CO_2$, CO, and SF_6 as tracers for recently added fossil fuel CO_2 in the atmosphere and implications for biological CO_2 exchange. *Geophys. Res. Lett.* **33**, L01817 (2006).
31. M. Lopez *et al*., CO, NOx and $^{13}CO_2$ as tracers for fossil fuel CO_2: Results from a pilot study in Paris during winter 2010. *Atmos. Chem. Phys.* **13**, 7343–7358 (2013).
32. I. Levin, S. Hammer, E. Eichelmann, F. R. Vogel, Verification of greenhouse gas emission reductions: The prospect of atmospheric monitoring in polluted areas. *Philos. Trans. A Math. Phys. Eng. Sci.* **369**, 1906–1924 (2011).
33. F. R. Vogel, S. Hammer, A. Steinhof, B. Kromer, I. Levin, Implication of weekly and diurnal 14C calibration on hourly estimates of CO-based fossil fuel CO_2 at a moderately polluted site in southwestern Germany. *Tellus B Chem. Phys. Meterol.* **62**, 512–520 (2010).
34. J. C. Turnbull *et al*., Toward quantification and source sector identification of fossil fuel CO_2 emissions from an urban area: Results from the INFLUX experiment. *J. Geophys. Res. Atmos.* **120**, 292–312 (2015).
35. J. C. Turnbull *et al*., Assessment of fossil fuel carbon dioxide and other anthropogenic trace gas emissions from airborne measurements over Sacramento, California in spring 2009. *Atmos. Chem. Phys.* **11**, 705–721 (2011).
36. C. Sweeney *et al*., Seasonal climatology of CO_2 across North America from aircraft measurements in the NOAA/ESRL Global Greenhouse Gas Reference Network. *J. Geophys. Res. Atmos.* **120**, 5155–5190 (2015).
37. J. C. Turnbull *et al*., A new high precision $^{14}CO_2$ time series for North American continental air. *J. Geophys. Res.* **112**, D11310 (2007).
38. S. J. Lehman *et al*., Allocation of terrestrial carbon sources using $^{14}CO_2$: Methods, measurement, and modeling. *Radiocarbon* **55**, 1484–1495 (2013).
39. V. Yadav *et al*., Spatio-temporally resolved methane fluxes from the Los Angeles megacity. *J. Geophys. Res. Atmos.* **124**, 5131–5148 (2019).
40. K. A. Masarie, P. P. Tans, Extension and integration of atmospheric carbon-dioxide data into a globally consistent measurement record. *J. Geophys. Res.* **100**, 11593–11610 (1995).
41. J. B. Miller, P. P. Tans, Calculating isotopic fractionation from atmospheric measurements at various scales. *Tellus B Chem. Phys. Meterol.* **55**, 207–214 (2003).
42. D. York, N. M. Evensen, M. L. Martínez, J. De Basabe Delgado, Unified equations for the slope, intercept, and standard errors of the best straight line. *Amer. J. Phys.* **72**, 367–375 (2004).
43. J. B. Miller *et al*., Linking emissions of fossil fuel CO_2 and other anthropogenic trace gases using atmospheric $^{14}CO_2$. *J. Geophys. Res.* **117**, D08302 (2012).
44. Y. T. Prairie, C. M. Duarte, Direct and indirect metabolic CO_2 release by humanity. *Biogeosciences* **4**, 215–217 (2007).
45. C. K. Gately, L. R. Hutyra, Large uncertainties in urban-scale carbon emissions. *J. Geophys. Res. Atmos.* **122**, 11242–11260 (2017).
46. C. Mini, T. S. Hogue, S. Pincetl, Estimation of residential outdoor water use in Los Angeles, California. *Landscapes Urban Plann.* **127**, 124–135 (2014).
47. E. B. Wetherley, J. P. McFadden, D. A. Roberts, Megacity-scale analysis of urban vegetation temperatures. *Remote Sens. Environ.* **213**, 18–33 (2018).
48. E. G. McPherson, J. R. Simpson, Q. Xiao, C. Wu, Million trees Los Angeles canopy cover and benefit assessment. *Landscapes Urban Plann.* **99**, 40–50 (2011).
49. M. Zimnoch *et al*., Partitioning of atmospheric carbon dioxide over Central Europe: Insights from combined measurements of CO_2 mixing ratios and their carbon isotope composition. *Isotopes Environ. Health Stud.* **48**, 421–433 (2012).